Title

Fully coupled two-phase flow and poromechanics modeling of coalbed methane recovery: Impact of geomechanics on production rate

Authors

Ma, Tianran
Rutqvist, Jonny
Oldenburg, Curtis M
et al.

Publication Date

2017-09-01

DOI

10.1016/j.jngse.2017.05.024

Peer reviewed

Fully Coupled Two-Phase Flow and Poromechanics Modeling of Coalbed Methane Recovery: Impact of Geomechanics on Production Rate

Tianran Ma [a, b, c], Jonny Rutqvist [c], Curtis M. Oldenburg [c], Weiqun Liu [a, b], Junguo Chen [d],

[a] Key Laboratory of Coal-based CO_2 Capture and Geological Storage, China University of Mining and Technology, Xuzhou, Jiangsu, China

[b] State Key Laboratory for Geomechanics and Deep Underground Engineering, China University of Mining and Technology, Xuzhou, Jiangsu, China

[c] Lawrence Berkeley National Laboratory, Earth Sciences Division, Berkeley, CA, USA

[d] College of Mining and Safety Engineering, Shandong University of Science and Technology, Qingdao, Shandong, China

Submitted manuscript accepted for publication in

Journal of Natural Gas Science and Engineering

https://doi.org/10.1016/j.jngse.2017.05.024

Final Version Published as:

Ma T., Rutqvist J., Oldenburg C.M., Liu W. and Chen J., Fully coupled two-phase flow and poromechanics modeling of coalbed methane recovery: Impact of geomechanics on production rate. *Journal of Natural Gas Science and Engineering* 45, 474- 486 (2017).

Abstract

This study presents development and application of a fully coupled two-phase (methane and water) and poromechanics numerical model for the analysis of geomechanical impact on coalbed methane (CBM) production. The model considers changes in two-phase fluid flow properties, i.e., coal porosity, permeability, water retention, and relative permeability curves through changes in cleat fractures induced by effective stress variations and desorption-induced shrinkage. The coupled simulator is first verified for poromechamics coupling and simulation parameters of a CBM reservoir model are calibrated by history matching against one year of CBM production field data from Shanxi Province, China. Then, the verified simulator and calibrated CBM reservoir model are used for predicting the impact of geomechanics on production rate for twenty years of continuous CBM production. The simulation results show that desorption-induced shrinkage is the dominant process in increasing permeability in the near wellbore region. Away from the wellbore, desorption-induced shrinkage is weaker and permeability is reduced by pressure depletion and increased effective stress. A sensitivity analysis shows that for coal with a higher sorption strain, a larger initial Young's modulus and smaller Poisson's ratio promote the enhancement of permeability as well as the production rate. Moreover, the conceptual model of the cleat system, whether dominated by vertical cleats with permeability correlated to horizontal stress or with permeability correlated to mean stress can have a significant impact on the predicted production rate. Overall, the study clearly demonstrates and confirms the critical importance of considering geomechanics for an accurate prediction of CBM production.

Keywords: CBM Recovery; Two-Phase Flow; Poromechanics; Coupled Model

Highlight:

(1) A fully coupled two-phase flow and poromechanics model for methane recovery

(2) Simulation parameters are calibrated by history matching against field data

(3) The geomechanics behaviors significantly affect the prediction of CBM production

2

1. Introduction

Coalbed methane (CBM), an unconventional gas resource, has caught considerable attention and interest, particularly in China, India, and Australia, because of the decline of conventional gas supplies and high demand of the global energy market (Moore, 2012; Thararoop, 2010; White et al., 2005). CBM has a unique reservoir mechanism compared to those of conventional gas and oil. Up to 98% of CBM within a reservoir is stored on the inner surface of the coal grains, or skeleton, in a matrix system by adsorption. The remainder is free gas that exists in the fractures of the cleat system. To extract CBM from the coal reservoir, large amounts of water must be pumped out (McKee and Bumb, 1987) in order to decrease the reservoir pressure down to the critical desorption pressure to release absorbed gas from the matrix into the cleat system. The different sizes of fractures in the cleat system act as the conduits for methane and water migration into the well. A typical CBM recovery with a vertical well is illustrated in Fig. 1.

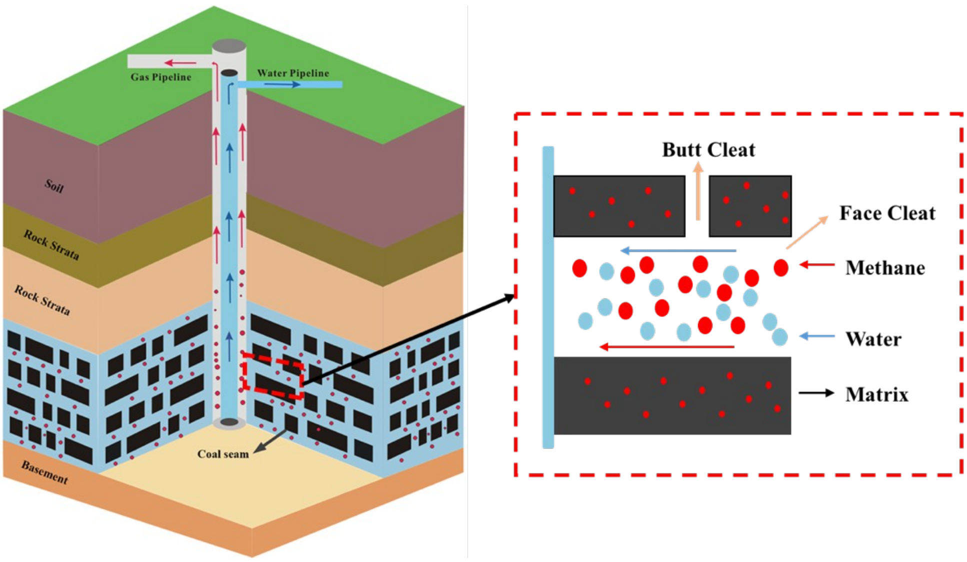

Fig. 1. Conceptual model of CBM and water production through a vertical well.

During the CBM production process, the variation in pore pressure causes a change in the stress state, which induces deformation of the reservoir. The permeability of coal is sensitive to stress changes and deformation (Clarkson et al., 2013; Wei and Zhang, 2013). As the pore pressure declines during production, the effective stress increases to narrow or even close the apertures of fractures in the cleat system and thus reduces coal permeability. Meanwhile, a shrinkage phenomenon occurs when methane desorbs from the surface of the matrix system. The shrinkage induced by gas desorption will enlarge the width of the cleat fractures, which enhances coal permeability. These coupled hydraulic and geomechanical processes can change permeability dramatically and will therefore have a significant impact on the evolution of CBM methane production.

A number of permeability models have been proposed to consider both the effects of pore pressure changes and shrinkage/swelling of the matrix system due to gas

3

desorption/adsorption. Gray (1987) was the first to propose a permeability model, which considers both the geomechanical deformation caused by pore pressure depletion and the shrinkage caused by gas desorption. Seidle et al.'s (1992) derived an exponential relationship between coal permeability and net confining stress. The well-known S&H model (Seidle and Huitt, 1995) assumes that permeability changes are solely controlled by a Langmuir-type swelling strain induced by gas desorption. Under uniaxial stress conditions, Palmer and Mansoori (1998) proposed a theoretical formulation for porosity and permeability change as a function of pore pressure. The P&M model was derived based on linear elasticity for porous rock deformation and sorption-induced strain, analogous to thermal expansion/contraction in a thermo-elasticity. Shi and Duncan (2004) developed a permeability model (S&D model), which also considers sorption-induced strain and pressure depletion under uniaxial strain conditions. The S&D model includes an exponential relationship between permeability and stress, similar to that of Seidle et al.'s (1992), but with permeability related to horizontal effective stress rather than mean effective stress. Cui and Bustin (2005) (C&B model) is equivalent to the S&D model, but mostly applied for the case when absolute permeability of the cleat system varies with the mean effective stress. Pan and Connell (2007) (P&C model) derived a theoretical model that describes adsorption-induced swelling resulting from the energy balance between the surface energy change from adsorption and the elastic energy change from the change in the solid skeleton.

In recent years models have been developed considering additional aspects such as internal swelling, multicomponent adorption, anisotropy, stress-dependent compressibility. Among those, Liu and Rutqvist (2009) considered the fracture–matrix interaction during coal-deformation processes based on the concept of internal swelling stress, which results from the partial separation of the matrix block by discontinuous fractures. Clarkson (Clarkson et al., 2010) proposed coupling the P&M and P&C model to extend the P&M model and incorporate multicomponent adsorption. Here, the P&M model refers to a more general expression, in which the sorption-induced volumetric strain is converted from the linear strain calculated in the P&C model. Moore (Moore et al., 2014) proposed an anisotropic permeability model to match the apparent exponential-type increase in permeability in the San Juan basin. The C&B and S&D models are both deduced with an assumption of a constant pore compressibility or bulk modulus; thus, initial porosity does not appear in both. Based on the C&B model, Ma et al. (2016) developed a new permeability model (M&R model) considering the variations in pore compressibility during pressure drawdown.

The recovery process of CBM is frequently simplified as a single phase gas flow process, neglecting the water existing on different scales of pores or injected into the coal seams for fracturing (Chen et al., 2013; Wang et al., 2012). Such simplification can have a strong influence on the predicted evolution of the CBM flow rate and cumulative production recovery. Saturation is one of most vital factors in determining the CBM production rate (Roadifer et al., 2003), as it affects the mobility, not only through variation in intrinsic permeability with swelling, but also through changes in the relative permeability. The impact

4

of swelling on mobility can be more significant in dry coal than coal saturated with water and gas (Moore, 2012). The free water that exists in the cleat system or the water that is injected during hydraulic fracturing affects the degree of saturation and capillary pressure that in turn affects the relative permeability of methane and water. The two well-known relatively permeability models of Brooks and Corey (1966) and Van Genuchten (1980), have been developed for unconsolidated and consolidated porous media, respectively. Laboratory experiments have been conducted to investigate the permeability of different coal with steady-state and unsteady-state methods (Durucan et al., 2013; Shen et al., 2011). In another approach, relative permeability has been determined by history matching with field production data (Zhou, 2012). Dynamic relative permeability models have also been proposed with consideration of the combined effects of stress changes and desorption-induced shrinkage of the matrix system (Xu et al., 2014). Chen et al. (2013) proposed a more direct relationship between effective mean stress changes and effective saturation, which was calibrated against experiments on different types of coal. In any case, the water retentions and relative permeability curves are a crucial multiphase flow property in predicting both the recovery rate of CBM and the amount of produced water (Clarkson et al., 2011).

In this paper, a mathematic model is developed to describe the coupled process of incorporating two-phase fluid flow and coal deformation caused by pore pressure and gas desorption during CBM production. The governing equations of the model are then implemented and solved in the multiphysics software COMSOL based on the finite element method. The performance and accuracy with respect to poromechanics are tested by a 1-D Terzaghi's consolidation problem. Then, a history matching of one year of CBM production data from the Shanxi Province, China, is performed to calibrate reservoir properties for the model. Finally, the same model is used in a sensitivity study to investigate the influences of geomechanics during 20 years of CBM and water production.

2. Theoretical Background

2.1. Fluid flow

The general mass balance equation for immiscible phases flow in a coal seam is given as

$$\frac{\partial m_\alpha}{\partial t} + \nabla \cdot \left(\rho_\alpha u_\alpha\right) = Q_\alpha \tag{1}$$

where Q_α is the flow sources or sinks ($\alpha = w \wedge g$ represent water and CBM, respectively).

The velocity u_α of fluid can be described by Darcy's law:

5

$$u_\alpha = \frac{-K\,k_{r\alpha}}{\mu_\alpha} \nabla p_\alpha \qquad (2)$$

where K and $k_{r\alpha}$ are the intrinsic and relative permeabilities, respectively. μ_α is the flow viscosity, and p_α is the pore pressure. m_α is the flow mass. The water mass is described as

$$m_w = S_w \rho_w \phi \qquad (3)$$

where S_w is the water saturation, ρ_w is the density of water and ϕ is the porosity of the cleat system.

The model assumes that coal is a single porosity and permeability medium, which implies that the methane absorbed on the surface of the coal grain diffuses instantaneously into the cleat without a desorption time lag. Thus, the methane mass in the fractures of the cleat system consists of free and adsorbed phases. The total mass is expressed as (Thararoop, 2010; Webb, 2011)

$$m_g = S_g \rho_g \phi + (1-\phi) \rho_{ga} \rho_c \frac{V_L p_g}{p_g + p_L} \qquad (4)$$

where ρ_c is the density of the coal seams and p_L and V_L are the Langmuir pressure and volume constant, respectively. To simplify the expression, this study assumes that $(1-\phi) \approx 1$. ρ_{ga} is the density of methane under standard conditions. This study also considers the compressibility of gas and water, which means that the density is not a constant that varies with pore pressure. The density is described by $\rho_\alpha = 1/C_\alpha (d\rho_\alpha / dp_\alpha)$, where C_α is the fluid compressibility, which is obtained from the NIST (NIST, n.d.).

Substituting Eqs. (3) and (4) into (1), the water flow equation can be rewritten as

$$\phi \rho_w S_w C_w \frac{\partial p_w}{\partial t} + \phi \rho_w \frac{S_w}{\partial t} + \rho_w S_w \frac{\partial \phi}{\partial t} + \nabla \cdot \left(-\rho_w \frac{K k_{rw}}{\mu_w} \nabla p_w \right) = Q_w \qquad (5)$$

The methane flow equation is expressed as

$$\rho_g S_g C_g \frac{\partial p_g}{\partial t} + \rho_{ga} \rho_c \frac{V_L p_L}{\left(p_g + p_L\right)^2} \frac{\partial p_g}{\partial t} + \phi \rho_g \frac{\partial S_g}{\partial t} + \rho_g S_g \frac{\partial \phi}{\partial t} + \nabla \cdot \left(- \rho_g \frac{K k_{rg}}{\mu_g} \right. \quad (6)$$

There are four variables (S_g , S_w , p_g and p_w) in the above equations. These variables cannot be solved without supplementary equations for saturation and capillary pressure.

$$S_w + S_g = 1 \quad (7)$$

$$p_c = p_g - p_w \quad (8)$$

where p_c is the capillary pressure, which is a function of saturation. The different functional relationships between capillary pressure and saturation and the relative permeability are adopted (Brooks and Corey, 1966; Leverett, 1941; Van Genuchten, 1980). In this study, capillary pressure and relative permeability are governed by the following functions (Pruess et al.,2012):

$$p_c = p_e (se)^{-1/\lambda} \quad (9)$$

$$k_{rg} = (1 - se)^2 (1 - se^2) \quad (10)$$

$$k_{rw} = \sqrt{se} \left\{ 1 - \left(1 - se^{1/m}\right)^m \right\}^2 \quad (11)$$

where p_e is the entry pressure and λ is a coefficient related to the pore size distribution. k_{rg} and k_{rw} are the relative permeabilities of gas and water, respectively. se is the effective saturation, defined as

$$se = \frac{S_w - S_{wr}}{1 - S_{wr} - S_{gr}} \quad (12)$$

where S_{wr} and S_{gr} are the residual saturations of water and gas, respectively, which change with the stress-induced porosity or permeability ratio (Chen et al., 2013):

$$S_{wr}=S_{wr0}\left(\frac{\phi}{\phi_0}\right)^{-n_{wr}}=S_{wr0}\left(\frac{\alpha}{\phi_0}+\frac{(\phi_0-\alpha)}{\phi_0}\exp\left(\frac{-\nabla\sigma'}{K}\right)\right)^{-n_{wr}} \tag{13}$$

$$S_{gr}=S_{gr0}\left(\frac{\phi}{\phi_0}\right)^{-n_{gr}}\left(\frac{\rho_g}{\rho_{ga}}\right)^{-1}=S_{gr0}\left(\frac{\alpha}{\phi_0}+\frac{(\phi_0-\alpha)}{\phi_0}\exp\left(\frac{-\nabla\sigma'}{K}\right)\right)^{-n_{gr}}\left(\frac{\rho_g}{\rho_{ga}}\right)^{-1} \tag{14}$$

where n_{wr} and n_{gr} are fitting parameters that are calculated by the experimental data. S_{wr0} and S_{gr0} are the initial values of the residual saturation in the water and gas phases, respectively. Hereto, the porosity, permeability, residual saturation, saturation and capillary pressure are all functions of the mean stress.

The production mass of water and methane on the well boundary are expressed as (Chen et al., 2013; Peaceman, 1978)

$$Q_w=\rho_w\frac{K k_{rw}(\overline{p}_w-p_{wb})}{\mu_w\left(\ln r_e-\ln r_w-\frac{3}{4}+S\right)} \tag{16}$$

$$Q_g=\rho_g\frac{K k_{rg}(\overline{p}_g-p_{wb})}{\mu_g\left(\ln r_e-\ln r_w-\frac{3}{4}+S\right)} \tag{17}$$

where p_{wb} is the bottom hole pressure (BHP), $\overline{p}_w$ and $\overline{p}_g$ are the average water and gas pressure in the reservoir, respectively, r_e is the drainage radius, r_w is the wellbore radius and S is the skin factor.

2.2. Stress-dependent porosity and permeability model

A new model of porosity/permeability was proposed in Ma et al. (2016) by considering the gas desorption/adsorption:

$$\phi=\alpha+(\phi_0-\alpha)\exp\left(\frac{-\Delta\sigma'}{K}\right) \tag{18}$$

$$\frac{k}{k_0}=\left(\frac{\phi}{\phi_0}\right)^3=\left\{\frac{\alpha}{\phi_0}+\frac{(\phi_0-\alpha)}{\phi_0}\exp\left(\frac{-\Delta\sigma'}{K}\right)\right\}^3 \tag{19}$$

Biot's coefficient α is assumed to be 1. From Eq. (18), the partial derivative of ϕ with respect to time is expressed as

$$\frac{\partial \phi}{\partial t} = \frac{-S}{K}\frac{\partial \sigma'}{\partial t} \tag{20}$$

where $S = (\phi_0 - \alpha)\exp\left(\frac{-\Delta\sigma'}{K}\right)$.

Substituting Eq. (20) into Eqs. (5) and (6), the model containing the governing equations for describing the effects of capillary pressure and coal deformation on porosity and permeability for water and gas flow in a coal seam is given as

$$\phi\rho_w S_w C_w \frac{\partial p_g}{\partial t} + \left(\phi\rho_w - \phi\rho_w S_w C_w d\,pc_{sw}\right)\frac{\partial S_w}{\partial t} + \nabla\cdot\left(-\rho_w \frac{K k_{rw}}{\mu_w}\left(\nabla p_g - \right.\right. \tag{21}$$

$$\left(\phi\rho_g S_g C_g + \rho_c \frac{V_L p_L}{\left(p_g + p_L\right)^2}\right)\frac{\partial p_g}{\partial t} - \phi\rho_g \frac{\partial S_w}{\partial t} + \nabla\cdot\left(-\rho_g \frac{K k_{rg}}{\mu_g}\nabla p_g\right) = \rho_g S_g \tag{22}$$

where $dpc_{sw} = \frac{\partial p_c}{\partial se}\frac{\partial se}{\partial S_w} = p_e\left(\frac{-1}{\lambda}\right)(se)^{\frac{-1}{\lambda}-1}$

2.3. Geomechanical model for coal deformation

Based on the constitutive relation of poro-elasticity and considering the methane-desorption-induced volumetric strain, the governing equation for deforming coal seams is expressed as follows (Rutqvist et al., 2001):

$$\sigma = \sigma' - \alpha I p = D : (\varepsilon - \varepsilon_s \delta) - \alpha I p \tag{23}$$

where σ and σ' are the total and effective stress (with tensile stress being a positive quantity), respectively, p is the pore pressure tensor, D is the tangential stiffness matrix and ε_s is the desorption-induced linear strain calculated by the Langmuir-type equation as

$$\varepsilon_s = \varepsilon_L \frac{p_g}{p_g + p_L} \tag{24}$$

where ε_L and p_L represent the Langmuir linear strain and Langmuir pressure constant, respectively. p is the mean pore pressure, expressed as

$$p = S_w p_w + S_g p_g = S_w \left(p_g - p_c \right) + S_g p_g = p_g - S_w p_c \tag{25}$$

2.4. Implementation of the numerical model

Eqs. (21), (22) and (23) are the final coupled equations for fluid flow and coal seam deformation. The three equations are implemented and solved with the COMSOL multiphysics software. A pre-arranged COMSOL geomechanics module is selected to solve the geomechanical part with Eq. (23). Two immiscible phase flows are implemented with Eqs. (21) and (22) using the COMSOL General Form PDE interface. In COMSOL, the General Form PDE equation for the primary variable **u** has the following expression:

$$e_a \frac{\partial^2 u}{\partial t^2} + d_a \frac{\partial u}{\partial t} + \nabla \cdot \Gamma = f \tag{26}$$

The two primary variables are

$$u = \begin{pmatrix} p_g \\ S_w \end{pmatrix} \tag{27}$$

In this study, pressure and saturation are chosen as the primary variables to achieve a relatively stable and robust convergence in COMSOL (Bjørnara and Aker, 2008). The PDE coefficients d_a, Γ and f are introduced as

$$d_a = \begin{bmatrix} \phi \rho_w S_w C_w & \left(\phi \rho_w - \phi \rho_w S_w C_w dpc_{sw} \right) \\ \phi \rho_g S_g C_g + \rho_{ga} \rho_c \dfrac{V_L p_L}{\left(p_g + p_L \right)^2} & -\phi \rho_g \end{bmatrix} \tag{28}$$

$$\Gamma_w = \begin{bmatrix} -\rho_w \dfrac{K k_{rw}}{\mu_w} \left(pgx - dpc_{sw} swx \right) \\ -\rho_w \dfrac{K k_{rw}}{\mu_w} \left(pgy - dpc_{sw} swy \right) \end{bmatrix} \Gamma_g = \begin{bmatrix} -\rho_g \dfrac{K k_{rg}}{\mu_g} pgx \\ -\rho_g \dfrac{K k_{rg}}{\mu_g} pgy \end{bmatrix} \tag{29}$$

10

$$f=\begin{bmatrix}\rho_w S_w \frac{S}{K}\frac{\partial \sigma'}{\partial t}\\ \rho_g S_g \frac{S}{K}\frac{\partial \sigma'}{\partial t}\end{bmatrix} \tag{30}$$

where pgx , pgy , swx and swy represent the partial derivative of gas pressure and water saturation in the x and y directions. The schematic of solving a coupled model of CO_2 flow and coal seam deformation in COMSOL Multiphysics is illustrated in Fig. 2.

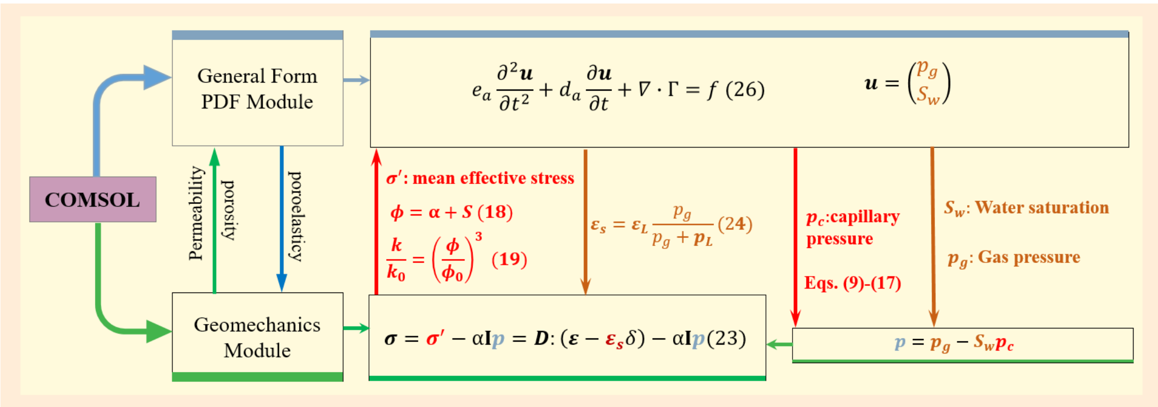

Fig. 2. Schematic of solving the coupled model of methane and water flow and coal defamation with COMSOL.

3. Model verification and calibration

3.1. Terzaghi's consolidation problem

The numerical solution and analytical solution of Terzaghi's consolidation problem were compared to verify the accuracy of our implementations and solution of the coupled equations in COMSOL Multiphysics. The analytical solution of the problem is presented by Verruijt (2013).

Fig. 3 describes the one-dimensional Terzaghi's consolidation problem. The sample is located at $z=0$, and its thickness is denoted by $2h=10$ m. The upper and lower are both fully drained, which ensures that the pore pressure remains zero along the two boundaries. A vertical load of $q=5\,MPa$ was applied at the top at $t=0$. Due to the sudden loading, the initial pore pressure is zero and instantaneously increases to the maximum. To solve Terzaghi's problem, a fine triangular element mesh is chosen to discretize the simulation region. The simulation parameters are listed in Table 1 (Yang et al., 2014).

11

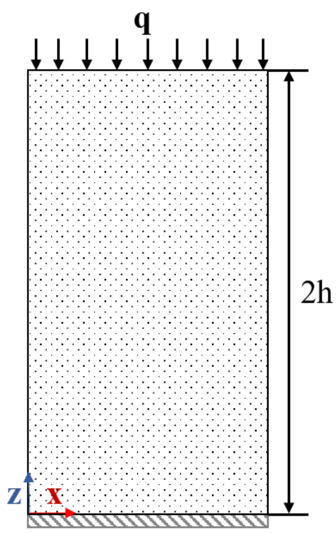

Fig. 3. Description of Terzaghi's consolidation problem.

Table 1 Simulation parameters for Terzaghi's consolidation problem.

Parameter	Value	Unit
Shear modulus of the rock	3×10^{10}	Pa
Compression modulus of the rock	5×10^{10}	Pa
Permeability	1×10^{-12}	m^2
Porosity	0.25	-
Compressibility of the fluid	1×10^{10}	Pa^{-1}
Viscosity of the fluid	1×10^{-3}	Pa · s

Fig. 4 presents the comparison between the analytical and numerical solutions when dimensionless time *t* = 0.2, 0.3 and 0.5. The results indicate that the discrete points of pore pressure extracted from COMSOL and the analytical solutions correspond well.

12

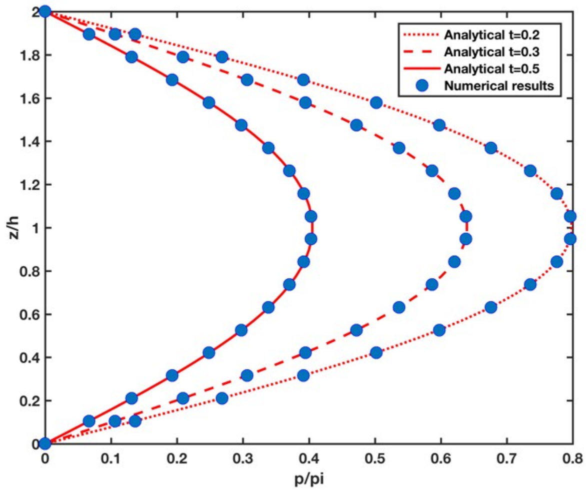

Fig. 4. Comparison of analytical and numerical results for the 1-D Terzaghi's consolidation problem.

3.2. History matching of field methane production

In this section, the relative permeability for the coupled simulation is calibrated by history matching of CBM production data from a vertical well in the south of Shanxi Province, China (Liu, 2013). Initially, approximately 320 m^3 of pressurized water was injected into the coal seam for hydraulic fracturing to improve connectivity to the well and increase the permeability of the reservoir. Then, during subsequent production, reservoir pressure was reduced to the critical desorption pressure to release adsorbed methane from the coal matrix into the cleat system. Both the methane and water was produced through the vertical well. Field history data of methane and water production from October 4th, 2007 to September 3rd, 2008, are used for model calibration in this study.

Fig. 5 presents a schematic of the model geometry and boundary conditions for the simulation. The reservoir extends laterally 600 by 600 m and is and 5 m thick with a well at the center. In the numerical simulation, a quarter of the reservoir and the vertical well is considered in a 2-D plain stress model. The initial pore pressure of the reservoir is approximately 4 MPa. The top of the coal seam is located at an average depth of 525.6 m and assumed to have a vertical boundary loading σ_v of -11.3 MPa corresponding to an overburden rock density of 2,300 kg/m^3. An isotropic initial horizontal stress calculated as $\sigma_h = \upsilon / (1-\upsilon) \sigma_z$ = -6.08 MPa, considering the condition of passive basin or zero lateral strain. Displacement constraints are assigned normal to the inner symmetric lateral boundaries, while constant stress are applied to the outer lateral boundaries. The parameters for history matching are summarized in Table 2.

13

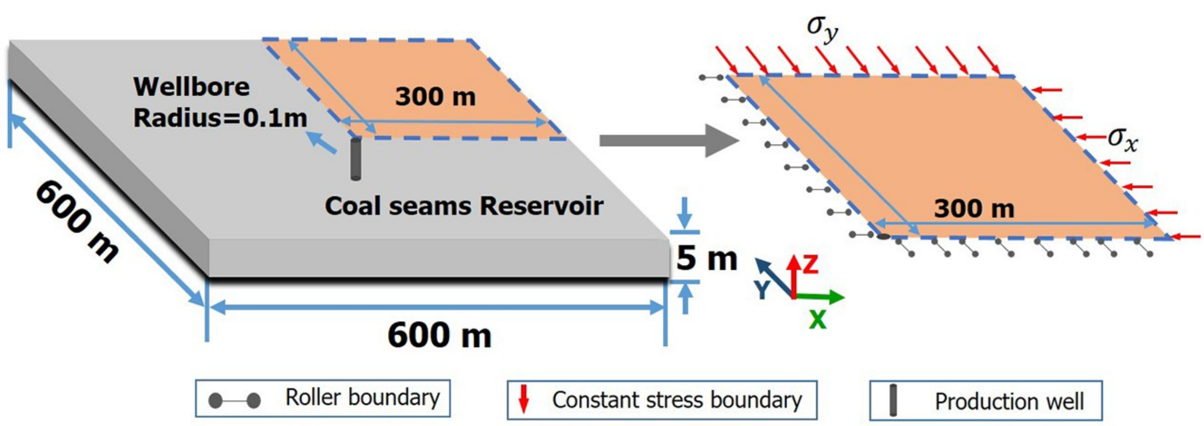

Fig. 5. Schematic of the geometric model for simulating the production of methane and water.

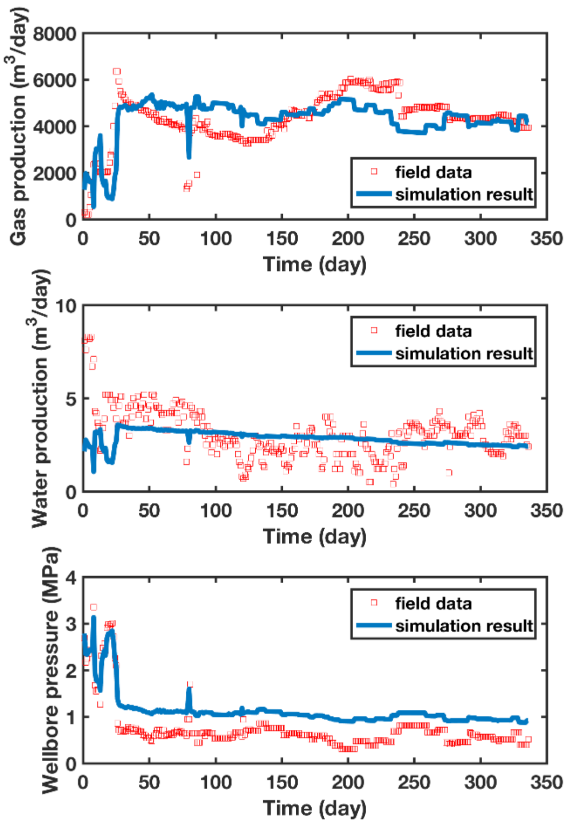

Fig. 6. Comparison between the simulation results and field data.

Table 2 Simulation parameters for history matching.

14

Parameters	Value	Unit
Drainage area	600 × 600	m^2
Coal seam thickness	5	m
Depth of coal seam	525.6	m
Coal density	1650	kg/m^3
Poisson's ratio of coal	0.35	
Elastic modulus of coal	3	GPa
Cleat permeability	1.628×10^{-13}	m^2
Cleat porosity	0.0302	
Biot coefficient	1	
Langmuir pressure constant	2.7	MPa
Langmuir volumetric constant	0.045	
Langmuir strain constant	0.03	
Initial reservoir pressure	3.99	MPa
Initial water saturation	0.592	
Viscosity of water	10^{-3}	Pa · s
Viscosity of gas	1.84×10^{-5}	Pa · s
Initial water density	1000	kg/m^3
Initial methane density	0.684	kg/m^3
Compressibility of water	1.38×10^{-5}	Pa^{-1}
Compressibility of methane	3.84×10^{-10}	Pa^{-1}
Capillary pressure model:	Eq. (9)	
Entry capillary pressure p_e	0.1	MPa
Coefficient λ	2.0	
Relative permeability model:	Eqs. (10) and (11)	
Coefficient m	0.6	
Residual saturation model:	Eqs. (13) and (14)	
Initial residual water saturation S_{wr0}	0.2	
Fitting parameter n_{wr}	0.49	
Initial residual methane saturation S_{gr0}	0.0	

The mass production rates of water and methane computed with Eqs. (16) and (17). are applied to the wellbore. Using the input data listed in Table 2, a good agreement is achieved between simulation results and field data (Fig. 6).

4. Modeling of HM effects on longer term CBM production

Having tested and calibrated the COMSOL CBM model, a sensitivity study is conducted to investigate coupled HM effects on longer-term CBM production. The same model grid is used as in the previous model calibration. The production is in this case modeled with a constant wellbore pressure at 0.1 MPa as this is numerically much more efficient for the

15

many simulations needed in the sensitivity study. All other parameters are those listed in Table 2. In the simulation, the BHP is linearly decreased down to 0.1 MPa in a short time and then kept constant for twenty years of production.

4.1 Base-case production modeling

Fig. 7 displays the spatial distribution of the pore pressure p, water saturation S_w, mean effective stress change $\Delta\sigma$ and permeability ratio k/k_0 after twenty years (7200 days) of production. The pressure and saturation decrease considerably all the way to the outer boundary, though largest decrease occurs close to the wellbore. Consistently, the mean effective stress change and permeability ratio are also the highest near the wellbore. The pore pressure and water saturation are below their initial state before production, which is because the drainage has already reached the outer lateral boundaries.

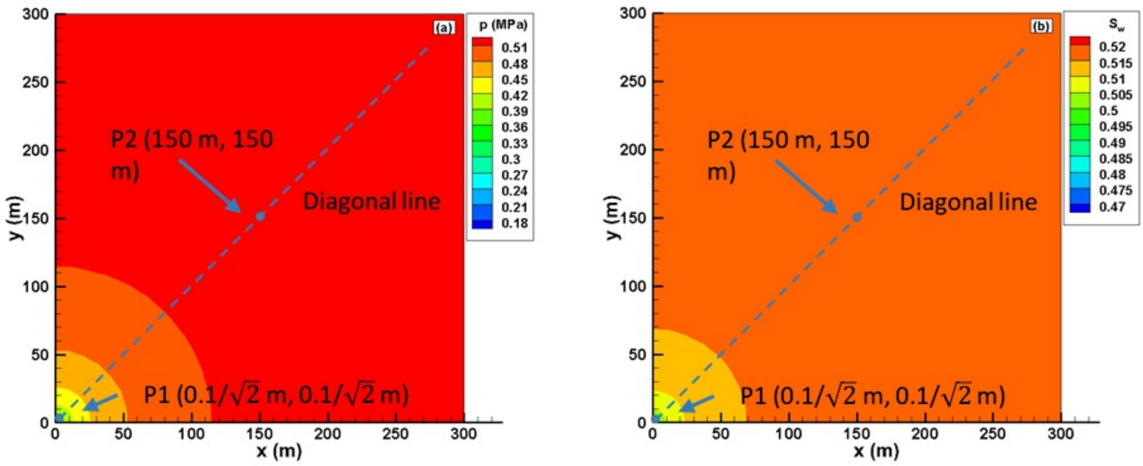

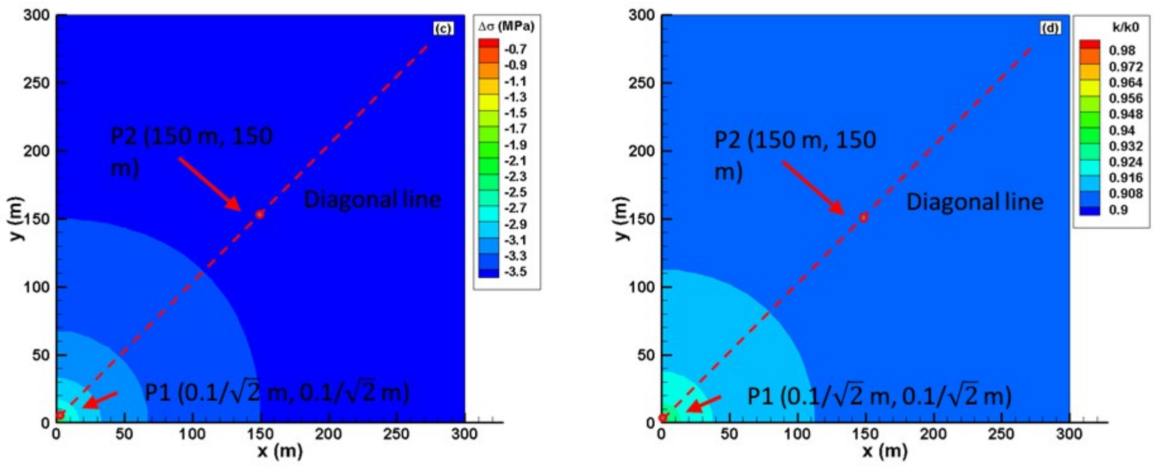

16

Fig. 7. Spatial distributions of the pore pressure p, water saturation S_w, mean effective stress change $\Delta\sigma$ and permeability ratio k/k_0 after twenty years of production.

The methane and water daily production rates are shown in Fig. 8. The gas production increases and approaches the peak in a short time as a result of continuous dewatering. Fig. 9 shows the temporal evolution of the four key parameters at monitoring points P1 and P2. P1 is located at the wellbore, whereas P2 (x= 150 m, y = 150 m) is located 150 $\sqrt{2}$ ≈ 212 m diagonal distance away from the production well. The pore pressure drops almost instantaneously at P1 as a result of the pressure drawdown applied at the well. The water saturation also decreases dramatically in a relatively short time because the majority of the water is extracted early on as a result of high initial water saturation and water relative permeability. The high water production prompts methane to migrate and accumulate near the wellbore. An almost instantaneous increase in effective mean stress occurs at P1 along with the initial pressure drop. This is followed by a gradual decrease in mean effective stress at both P1 and P2, which is a result of shrinkage as methane in desorbed from the rock matrix.

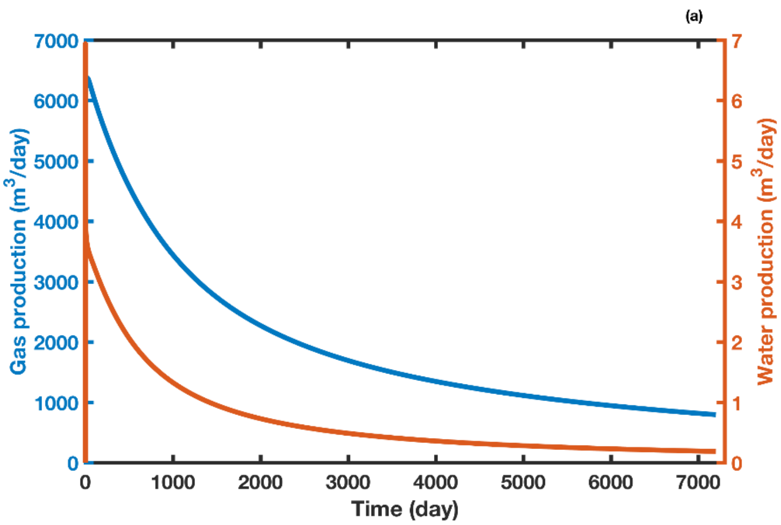

Fig. 8. CBM and water production rate versus time.

At P1, an initial increase in permeability by a factor of 1.3 is the net effect of an increased effective stress and rapid desorption shrinkage. Thereafter, the permeability at P1 decreases gradually as the shrinkage effect weakens along with continuous increased effective stress. At P2. a decrease in the mean effective stress σ with the drawdown of pore pressure and desorption shrinkage causes a reduction in the permeability of the cleat system.

17

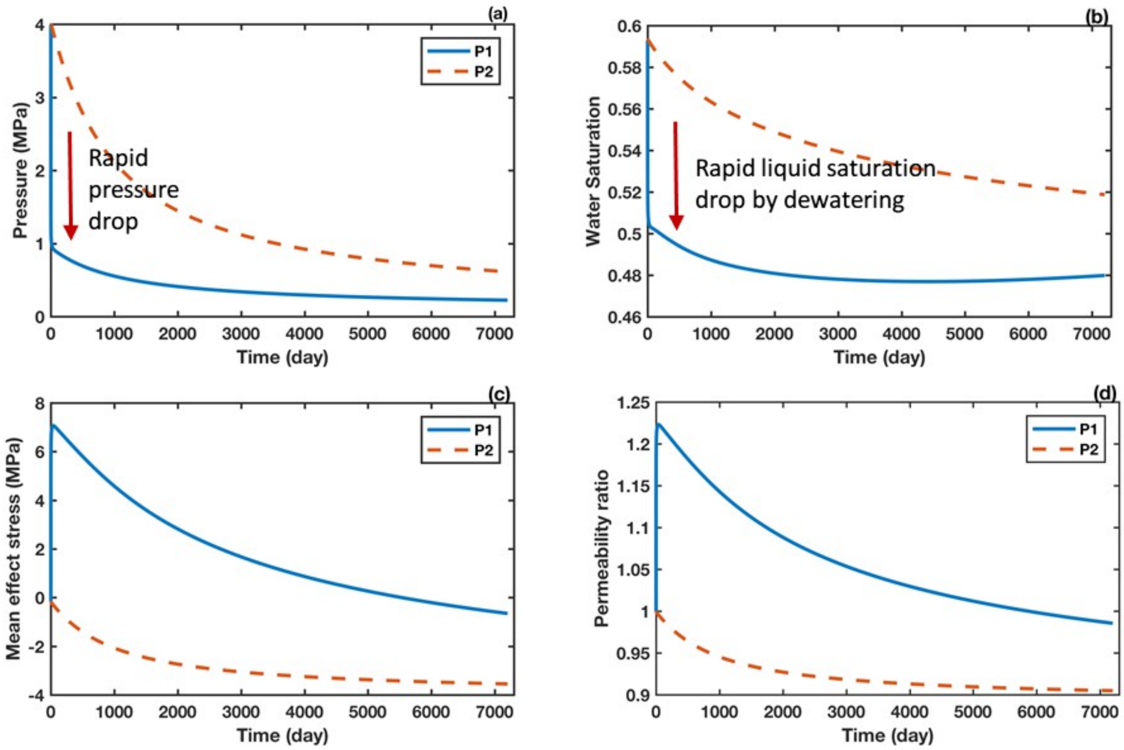

Fig. 9. Temporal evolution of the pore pressure p, water saturation S_w, mean effective stress chang□ σ and permeability ratio k/k_0 at monitoring points P1 and P2.

4.2. Production with different permeability models

The permeability model proposed in Ma et al., (2016), and the three other widely used models of P&M, S&D, and C&B are applied. The production profiles of CBM and water and the evolution of permeability are predicted, as shown in Fig. 10. The comparison indicates that the production of methane and water and the permeability ratio show similar variation. However, the permeability values obtained with the S&D model are significantly higher than those obtained with the other models. This phenomenon can be explained by the fact that under the S&D model, the dominant controlling effect of permeability variation during pressure depletion is the horizontal effective stress, whereas the other three models adopt the mean effective stress. The S&D model can reflect a greater increase in permeability as the pore pressure approaches a minimum (Thararoop, 2010). The results estimated from the C&B and P&M models and the model proposed in Ma et al. (2016) have subtle differences, which results from the different simplifications in each model. The C&B model assumes that the bulk modulus of the pores is constant, whereas the P&M model is deduced for low-porosity (less than 1%) coal seams.

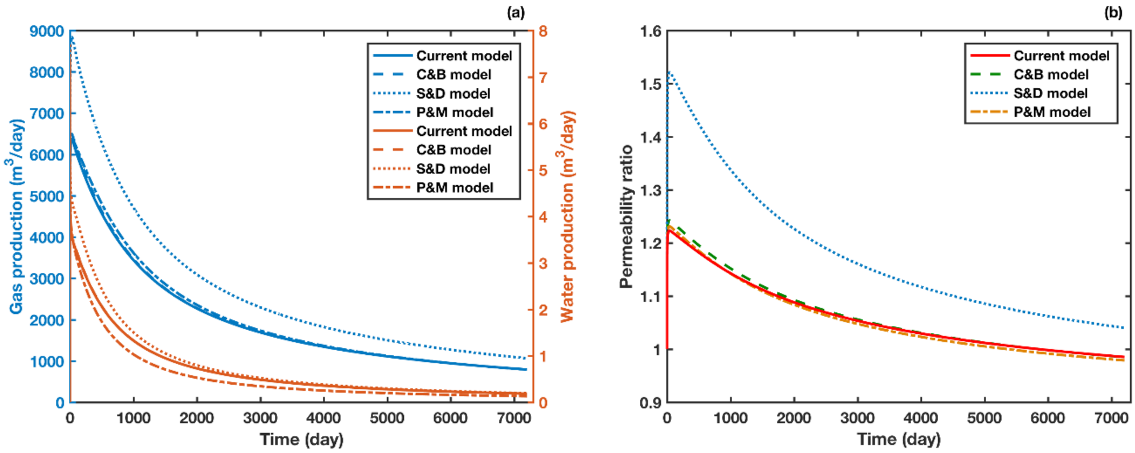

Fig. 10. (a) CBM and water production rate **(b)** permeability ratio versus time with different permeability models.

4.3. Effect of shrinkage and coal deformation

The effect of shrinkage and coal deformation are investigated with the results shown in Fig. 11.. The model assuming a constant permeability and porosity produces a lower rate than the coupled model. The highest and lowest production rates are predicted within the models that do not consider the effect of pore pressure and shrinkage on permeability. As noted above, depressurization releases the methane absorbed on the skeleton of the matrix system, which induces shrinkage and thus widens the aperture of fracture in the cleat system. This gives rise to the enhancement of its corresponding permeability, as well as the water and methane rate of production, whereas the pore pressure has the reverse effects. Moreover, the model without pore pressure displays a stronger permeability variationthe model without shrinkage, which also indicates the dominance of shrinkage-induced strain.

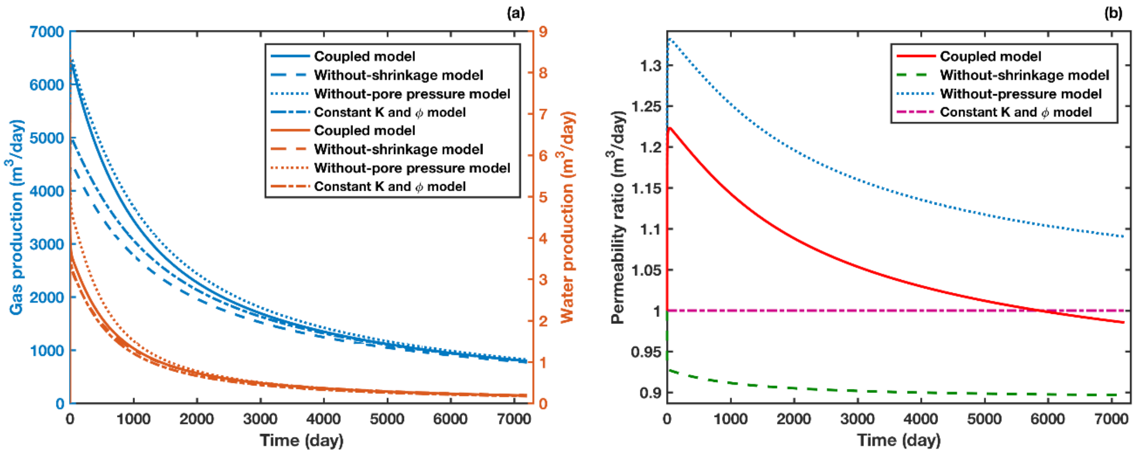

Fig. 11. (a) CBM and water production rate (b) permeability ratio versus time for four different cases

4.3. Effect of sorption strain constants

Fig. 12 presents the CBM and water production rates and the change in permeability with different Langmuir strain constants ε_L of 0.01, 0.03, 0.05. The production curves shown in

19

Fig. 12a follow similar trend. However, the production rate of methane is higher in the coal with a larger sorption strain, which is attributed to stronger shrinkage effects on the fracture apertures, thus resulting in a larger increase in permeability, as shown in Fig. 12b. The permeability increases to approximately 1.7 times the initial value in the case with a high ε_L . The decrease in ε_L will weaken the dominance of shrinkage, and as expected, the permeability has only a small and brief enhancement in that case.

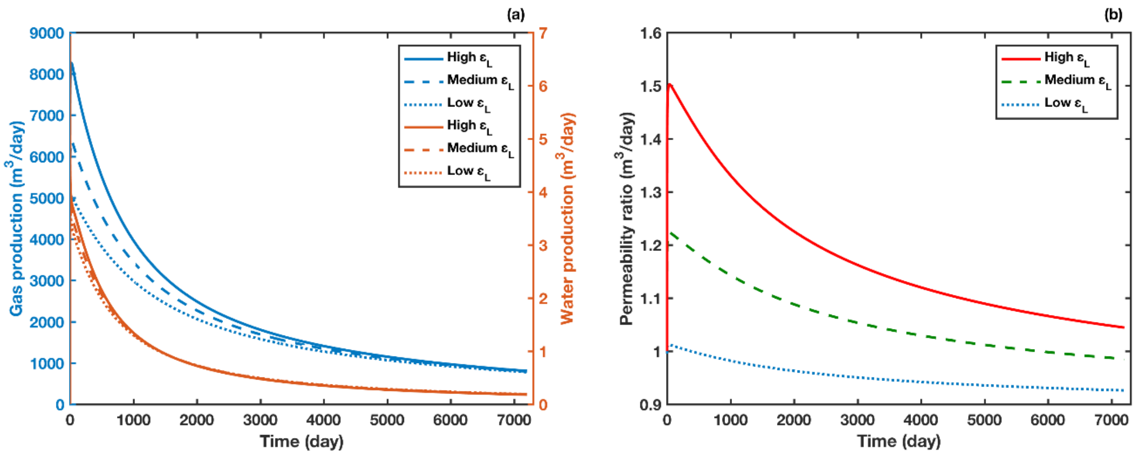

Fig. 12. Impacts of different Langmuir strain constants ε_L =0.01, 0.03, and 0.05 on (a) CBM and water production rate (b) permeability ratio.

4.4. Effect of Young's modulus and Poisson's ratio

The Young's modulus and Poisson's ratio ν are two of the most important parameters for coal deformation. The influences of *E* and ν are investigated in this section. The *E* and ν values for coal with low, medium and high deformability are listed in Table 3 (Balan and Gumrah, 2009).

Table 3 Different Young's moduli and Poisson's ratios.

Cases	*E* (GPa)	υ
Low	0.85	0.21
Medium	4.1	0.35
High	6.10	0.48

The methane and gas production rates for three different Young's moduli are compared in Fig. 13a. The results show that greater production is obtained for the coal seam with a higher Young's modulus. The increase in the modulus will reduce the compressibility of the cleat and suppress the influence of pore pressure on permeability. If the Young's modulus of the coal seam increases to infinity, the predicted production would be equivalent to the model without consideration of the deformation induced by the pore pressure in Fig. 11a.

20

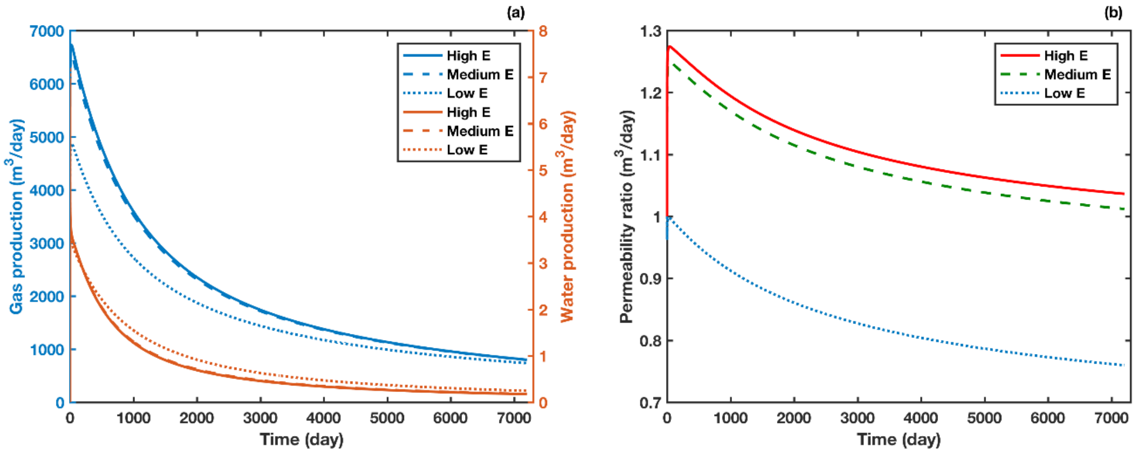

Fig. 13. Impacts of Young's modulus on the (a) CBM and water production rate (b) permeability ratio.

Fig. 14a shows the influences of Poisson's ratio during production. The model predicts that the production rate is higher for a coal seam with a higher Poisson's ratio. Poisson's ratio affects both shrinkage and pressure-induced deformation; thus, the boundary conditions or even the initial value for simulation parameters would result in distinct conclusions for a different permeability model. Coal with a higher Poisson's ratio results in a higher production rate with the C&B and G&C models but lower values in the S&D and P&M models (Cui and Bustin, 2005; Gu and Chalaturnyk, 2005; Zulkarnain, 2005). Thus, our results show significant influence of Poisson's ratio, which somewhat contradicts finding by Balan and Gumrah (2009) who stateed that Poisson's ratio does not affect CBM recovery.

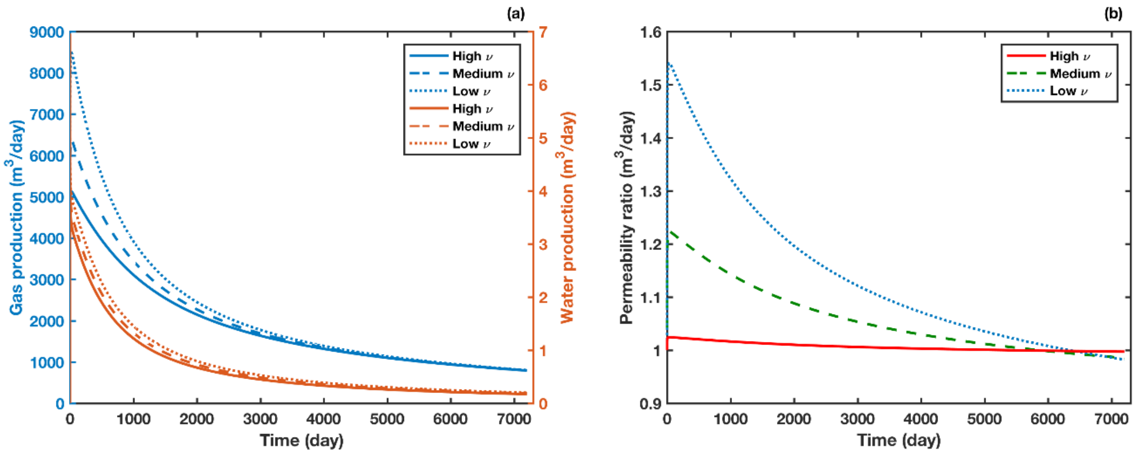

Fig. 14. Impacts of Poisson's ratio on the (a) CBM and water production rate (b) permeability ratio.

5. Summary

This study presents development and application of a fully coupled two-phase (methane and water) and poromechanics numerical model for the analysis of geomechanical impact on coalbed methane (CBM) production. The model considers changes coal porosity, permeability, water retention, and relative permeability curves through changes in cleat fractures induced by effective stress variations and desorption-induced shrinkage. The coupled simulator was first verified for poromechamics coupling and simulation parameters of a CBM reservoir model were calibrated by history matching against one year of CBM production field data from Shanxi Province, China. Then, the verified simulator and calibrated CBM reservoir model were used for predicting the impact of geomechanics on production rate for twenty years of continuous CBM production.

The simulation results show that the production reduces the pore pressure and water saturation, particularly near the wellbore. The depressurization increases the effective stress and thus decreases the intrinsic permeability away from the well. However, the permeability near the wellbore exhibits an increase early on because of a pronounced shrinkage-induced strain by gas desorption. Among different permeability models tested, the S&D predicts distinctly larger permeability values because of the assumption that the permeability is a function of the horizontal effective stress, rather than the mean effective stress.

Ignoring the influences of pore pressure or matrix shrinkage-induced strain may lead to over- or under-estimated prediction of CBM production rate. The sensitive results indicate that for coal with a high sorption strain, a larger initial Young’s modulus and smaller Poisson’s ratio promote the enhancement of permeability and hence results in a higher production rate. Overall, the simulation results show that geomechanical behavior has a significant impact, which is important to consider for more accurate prediction CBM production.

Acknowledgments

Tianran Ma would like to thank Tore Ingvald Bjornara and Dong Chen for their helpful discussions on the simulation. This study was supported by Special Subject Grant of National “973” Basic Research Program of China (No. 2015CB251602 and No.2009CB219605), National Natural Science Foundation of China (No. 41074040 and No. 50774083), Jiangsu Natural Science Foundation (No. BK20141125), Chinese Program for New Century Excellent Talents in University (No. NCET-07-0803) and Opening Fund (NO. 2016A01). The work was funded in part by the U.S. Department of Energy under contract no. DE-AC02-05CH11231. Special thanks to the anonymous reviewers for their valuable comments.

References

Balan, H.O., Gumrah, F., 2009. Assessment of shrinkage–swelling influences in coal seams using rank-dependent physical coal properties. Int. J. Coal Geol. 77, 203–213.

Bjørnara, T.I., Aker, E., 2008. Comparing equations for two-phase fluid flow in porous media, in: Proceedings of the Conference on COMSOL, Hannover.

Brooks, R.H., Corey, A.T., 1966. Properties of porous media affecting fluid flow. J. Irrig. Drain Eng. 92, 61–90.

Chen, D., Pan, Z., Liu, J., Connell, L.D., 2013. An improved relative permeability model for coal reservoirs. Int. J. Coal Geol. 109–110, 45–57.

 22

Clarkson, C.R., Pan, Z., Palmer, I.D., Harpalani, S., 2010. Predicting sorption-induced strain and permeability increase with depletion for coalbed-methane reservoirs. SPE J. 15, 152–159.

Clarkson, C.R., Qanbari, F., 2015. Transient flow analysis and partial water relative permeability curve derivation for low permeability undersaturated coalbed methane wells. Int. J. Coal Geol. 152, 110–124.

Clarkson, C.R., Qanbari, F., Nobakht, M., Heffner, L., 2013. Incorporating geomechanical and dynamic hydraulic-fracture-property changes into rate-transient analysis: example from the haynesville shale. SPE Reserv. Eval. Eng. 16, 303–316.

Clarkson, C.R., Rahmanian, M., Kantzas, A., Morad, K., 2011. Relative permeability of CBM reservoirs: controls on curve shape. Int. J. Coal Geol. 88, 204–217.

Cui, X., Bustin, R.M., 2005. Volumetric strain associated with methane desorption and its impact on coalbed gas production from deep coal seams. AAPG Bull. 89, 1181–1202.

Durucan, S., Ahsan, M., Syed, A., Shi, J.-Q., Korre, A., 2013. Two phase relative permeability of gas and water in coal for enhanced coalbed methane recovery and CO_2 storage. Energy Proced. 37, 6730–6737.

Liu, A.H, 2013. Dynamic change features of water chemistry during coal reservior drainage and physical simulation of cbm desorption at fixed pressures and flow in southern qinshui basin. (Doctoral Dissertation), geological resources and geological engineering. China University of Mining and Technology.

Gray, I., 1987. Reservoir engineering in coal seams. Part 1: the physical process of gas storage and movement in coal seams. SPE Reserv. Eng. 2, 28–34.

Gu, F., Chalaturnyk, R.J., 2005. Sensitivity study of coalbed methane production with reservoir and geomechanic coupling simulation. J. Can. Pet. Technol. 44.

Gu, F., Chalaturnyk, R.J., 2006. Numerical simulation of stress and strain due to gas sorption/desorption and their effects on *in situ* permeability of coalbeds. J. Can. Pet. Technol. 44.

Leverett, M.C., 1941. Capillary behavior in porous solids. Trans. AIME 142, 152–169.

Liu, H.-H., Rutqvist, J., 2009. A new coal-permeability model: internal swelling stress and fracture–matrix interaction. Trans. Porous Media 82, 157–171.

Ma, T., Rutqvist, J., Weiqun, L., Zhu, L., Kunhwi, K., 2016. Modeling of CO_2 sequestration in coal seams: role of CO_2-induced coal softening on injectivity, storage efficiency and caprock deformation. Sumbit to greenhouse gases. Science and Technology.

McKee, C.R., Bumb, A.C., 1987. Flow-testing coalbed methane production wells in the presence of water and gas. SPE Form. Eval. 2, 599–608.

Moore, R., Palmer, I., Higgs, N., 2014. Anisotropic model for permeability change in coalbed methane wells, in: SPE Western North American and Rocky Mountain Joint Meeting, Society of Petroleum Engineers, Denver, Colorado.

Moore, T.A., 2012. Coalbed methane: a review. Int. J. Coal Geol. 101, 36–81.

NIST, n.d. Thermophysical properties of fluid systems.

Palmer, I., 2009. Permeability changes in coal: analytical modeling. Int. J. Coal Geol. 77, 119–126.

23

Palmer, I., Mansoori, J., 1998. How permeability depends on stress and pore pressure in coalbeds: a new model. SPE Reserv. Eval. Eng. 1, 539–544.

Pan, Z., Connell, L.D., 2007. A theoretical model for gas adsorption-induced coal swelling. Int. J. Coal Geol. 69, 243–252.

Peaceman, D.W., 1978. Interpretation of well-block pressures in numerical reservoir simulation (includes associated paper 6988). Soc. Pet. Eng. J. 18, 183–194.

Pruess, K., Oldenburg, C.M., Moridis, G.J., 2012. TOUGH2 User's Guide Version 2. Lawrence Berkeley National Laboratory, Berkeley, CA.

Roadifer, R.D., Moore, T.R., Raterman, K.T., Farnan, R.A., Crabtree, B.J., 2003. Coalbed methane parametric study: what's really important to production and when? in: SPE Annual Technical Conference and Exhibition, Society of Petroleum Engineers, Denver, CO.

Rutqvist, J., Börgesson, L., Chijimatsu, M., Kobayashi, A., Jing, L., Nguyen, T.S., Noorishad, J., Tsang, C.F., 2001. Thermohydromechanics of partially saturated geological media: governing equations and formulation of four finite element models. Int. J. Rock Mech. Mining Sci. 38, 105–127.

Seidle, J.P., Jeansonne, M.W., Erickson, D.J., 1992. Application of matchstick geometry to stress dependent permeability in coals, in: SPE Rocky Mountain Regional Meeting, Society of Petroleum Engineers, Casper, Wyoming.

Seidle, J.R., Huitt, L.G., 1995. Experimental measurement of coal matrix shrinkage due to gas desorption and implications for cleat permeability increases, in: International Meeting on Petroleum Engineering, Society of Petroleum Engineers, Beijing.

Shen, J., Qin, Y., Wang, G.X., Fu, X., Wei, C., Lei, B., 2011. Relative permeabilities of gas and water for different rank coals. Int. J. Coal Geol. 86, 266–275.

Shi, J.Q., Durucan, S., 2004. Drawdown induced changes in permeability of coalbeds: a new interpretation of the reservoir response to primary recovery. Trans. Porous Media 56, 1–16.

Thararoop, P., 2010. Development of a Multi-mechanistic, Dual-porosity, Dual-permeability Numerical Flow Model for Coalbed Methane Reservoirs accounting for Coal Shrinkage and Swelling Effects (Doctoral Dissertation), Petroleum and Mineral Engineering. Penn State University.

Van Genuchten, M.T., 1980. A closed-form equation for predicting the hydraulic conductivity of unsaturated soils. Soil Sci. Soc. Am. J. 44, 892–898.

Verruijt, A., 2013. Theory and Problems of Poroelasticity. Delft University of Technology, Delft.

Wang, J.G., Kabir, A., Liu, J., Chen, Z., 2012. Effects of non-Darcy flow on the performance of coal seam gas wells. Int. J. Coal Geol. 93, 62–74.

Webb, S.W., 2011. EOS7C-ECBM Version 1.0: Additions for Enhanced Coal Bed Methane Including the Dusty Gas Model. Canyon Ridge Consulting Report, Sandia Park, NM.

Wei, Z., Zhang, D., 2013. A fully coupled multiphase multicomponent flow and geomechanics model for enhanced coalbed-methane recovery and CO_2 storage. SPE J. 18, 448–467.

 24

White, C.M., Smith, D.H., Jones, K.L., Goodman, A.L., Jikich, S.A., LaCount, R.B., DuBose, S.B., Ozdemir, E., Morsi, B.I., Schroeder, K.T., 2005. Sequestration of carbon dioxide in coal with enhanced coalbed methane recovery: a review. Energy Fuels 19, 659–724.

Xu, H., Tang, D.Z., Tang, S.H., Zhao, J.L., Meng, Y.J., Tao, S., 2014. A dynamic prediction model for gas–water effective permeability based on coalbed methane production data. Int. J. Coal Geol. 121, 44–52.

Yang, D., Moridis, G.J., Blasingame, T.A., 2014. A fully coupled multiphase flow and geomechanics solver for highly heterogeneous porous media. J. Comput. Appl. Math. 270, 417–432.

Zhou, F., 2012. History matching and production prediction of a horizontal coalbed methane well. J. Pet. Sci. Eng. 96–97, 22–36.

Zulkarnain, I., 2005. Simulation Study of the Effect of Well Spacing, Effect of Permeability Anisotropy, and Effect of Palmer and Mansoori Model on Coalbed Methane Production. Master’s thesis, Texas A&M University.

25